



A New Type of 3D Printing Molding Equipment: Overall Structural Design and the Numerical Simulation for the Flow Field Characteristics of its Screw Module

Haiqing Bai^{1,2} · Wang Qin¹ · Shikui Jia^{1,2} · Li Ren¹ · Yiwei An¹ · Jun Bao¹

Received: 19 October 2020 / Revised: 22 April 2021 / Accepted: 5 July 2021 / Published online: 11 August 2021
© Korean Society for Precision Engineering 2021

Abstract

Considering the problems faced by Fused Deposition Modeling (FDM) 3D printing equipment, including limited consumables choices and unstable extrusion rate as well as difficult prints precision control, etc., a new type of 3D printing molding equipment was designed following the current screw extrusion technology combined with 3D printing molding mechanism. Also, the optimal matching relation between the rotational speed of the screw, which is the core of the equipment, and the feed rate of the nozzle was determined. The POLYFLOW, the software of finite element numerical simulation, was employed for analyzing the performance of the screw module under different working conditions. The result revealed that the outlet fluid pressure derived from the theoretical calculation (1.48 MPa) was close to the simulation value of 1.51 MPa, and the volumetric flow rate at the outlet derived from theoretical calculation $3.51 \times 10^{-8} (\text{m}^3/\text{s})$ was close to the value obtained from simulation ($3.18 \times 10^{-8} (\text{m}^3/\text{s})$). Those findings indicated that the material could be extruded at a constant output rate; with the increase of the screw lead size, the pressure build-up capacity of screw improved, and the pressure fluctuation and velocity change became more intensive; therefore, the lead within the range of 24~36 mm should be the suitable choice for the application in actual production; the reduction of the rational speed resulted a lower shear rate, therefore, the screw rotational speed should be optimized within the reasonable range of 8~15r/min ($N_{\max} \sim N_{\min}$) and the feed rate of nozzle should be selected within the range of 1043.33~746.24 mm/min ($V_{F\max} \sim V_{F\min}$).

Keywords 3D printing molding equipment · End face profile · Twin-screw extrusion · POLYFLOW · Finite element analysis · Flow field characteristics

1 Introduction

With the rapid advancement of 3D printing, Fused Deposition Modeling (FDM) has emerged as an important rapid prototyping technology [1, 2]. Among all, the FDM linear plastic 3D printer has widespread applications owing to its high printing precision, convenient operation, and other competitiveness. Yet it is difficult to be further promoted due to restrictions regarding the extrusion pressure in the

die, consumables cost, materials categories, product performance, etc. To evade these hurdles, screw extrusion-based 3D printers are commonly adopted as the technical solution, especially for open-source desktop devices, to the problems in silk printing [3].

Globally, scholars have conducted relevant researches on the new technologies in 3D printing and achieved progress for the current stage. In terms of the structural design of the molding system: Thermwood [4] introduced a new type of extrusion systems of the 3D printer for polymers, which improved the deposition rate for the granular raw materials by applying a single-screw extruder; Z. C. Silveira et al. [5] explored the feasibility of mini-head screw extrusion technology to be adopted in desktop fused deposition 3D printers; Wang Tianming et al. [6] proposed a new type of extruding deposition head based on the features of the screw extrusion technology and other established nozzle technologies. In case of the mixing performance of the

✉ Wang Qin
2832591786@qq.com

¹ School of Mechanical Engineering, Shaanxi University of Technology, No. 1, East First Ring Road, Hantai District, Hanzhong City 723000, Shaanxi Province, China

² Shaanxi Key Laboratory of Industrial Automation, Hanzhong 723000, Shaanxi, China

twin-screw extrusion: by a mixing analysis for differently-configured assembled screw in a modular intermeshing co-rotating twin-screw extruder ZSK60, Hu Dongdong et al. [7] obtained the mixing performances of distribution and dispersion for assembled screw; L. Orefice et al. [8] studied the volumetric flow rate of granular materials in the horizontal screw conveyor and observed that the volumetric throughput was linearly proportional to the screw's rotational speed yet its dependence on the filling level was non-linear; T. Villmow et al. [9] studied the effect of the screw rotational speed and the feed rate on residence time and mechanical properties, and found that the processing conditions would have an impact on both the residence time of extruded materials and the material dispersion. Arash Sarhangi Fard et al. [10] analyzed the screw modules with the different geometric structures in their mixing performances and found that as the size of the clearance between the two screws and between the screw and the barrel increased, the axial mixing was enhanced. In terms of molding process parameters: the effect of processing parameters on the mechanical properties and dimensional accuracy of FDM products were investigated by S. Aslanzadeh et al. [11], which revealed the factors affecting the mechanical properties of printed products; Shushu Wang [12] studied the impact of different FDM processing parameters on the tribological behavior of printed products and the wear mechanism behind such influence, a research which provided useful practical guidance for the selection of FDM manufacturing parameters to enrich the tribological performance; C. C. Spackman et al. [13] systematically analyzed the influence of key process parameters on the tensile properties and failure mechanisms of 3D-printed FrSCs; exploring the influence of FDM processing parameters on processing time and power consumption, V. Lunetto [14] experimentally substantiated the fact that the proposed models were able to predict the power consumption of the complete process; M. Rackl et al. [15] studied the effect of processing parameters on the mass flow characteristics at the outlet of the screw conveyor- a research visualized by high-resolution cameras.

Although the screw extrusion-based 3D printing technology has been explored, the majority focuses on the conical screw and traditional single screw. However, molding equipment of such type still has problems in print quality, printing efficiency, energy dissipation, etc. In comparison, an effective solution to the above glitches is provided by the advent of twin-screw extrusion technology. Its characteristics (great mixing performance, excellent shearing plasticization, self-cleaning function, strong productivity, etc.) are widely deployed in extrusion equipment. Twin-screw, whose complex geometric configurations have a vital impact on the extrusion performance of polymeric material, serves as the core module of the extrusion system. Unreasonable design of screw may fail to build-up pressure in the extrusion process and incur fluctuation in the flow field, velocity, pressure,

etc., thus affecting the extrusion stability and printed-product quality. Therefore, it is essential to elucidate the twin-screw structure and extrusion process of the new 3D printer.

This study integrated the techniques of screw extrusion and FDM to design a new type of desktop double-screw extrusion-based 3D printing molding equipment. Furthermore, according to the printer's structural characteristics and technical requirements, it determined the basic structural parameters of the double-screw, the core of the extrusion system. The optimal matching relation between the screw rotational speed and the feed rate had been obtained from there. Moreover, the analysis of the isothermal transient flowing of polymer in the screw channel was made to explore the regularity of the screw effect on the melt conveying performance under different geometric parameters, which authenticated the rationality of the structural design of screw and prepared precondition for the smooth extrusion molding of polymeric materials.

2 The Working Mechanism and Motion Analysis of the New 3D Printing Molding Equipment

2.1 The Working Mechanism of Screw Extrusion-Based 3D Printing Molding Equipment

An externally heated screw extrusion system was adopted by this new type of 3D printing molding equipment to realize the melting plasticization of printing materials. In this process, the materials passed through three reaction areas in the order of feeding section, compression section, and homogenization section.

Materials were fed from the hopper into the barrel. As a joint effect of positive displacement conveying, abrasion, and viscous dragging of the counter-rotating twin-screw, the loose solid was gradually compressed as being conveyed forward. The heat from both the external heating system and the internal viscous dissipation transformed these solids into the melts, which passed through extrusion dies at constant pressure, output rate, and temperature as extruded by the nozzle. Printed products were shaped and obtained after the extruded materials were cooled. The process is illustrated in Fig. 1.

2.2 Design for the Work System of this New 3D Printing Molding Equipment

Based on the analysis of the working mechanism of the new screw extrusion 3D printing molding equipment as shown in Fig. 2, the 3D printing molding system is determined to be composed of three parts: the numerical control system, X–Y–Z three-dimensional movement system and material melt extrusion conveying system. The flow diagram of the equipment working system is shown in Fig. 2:

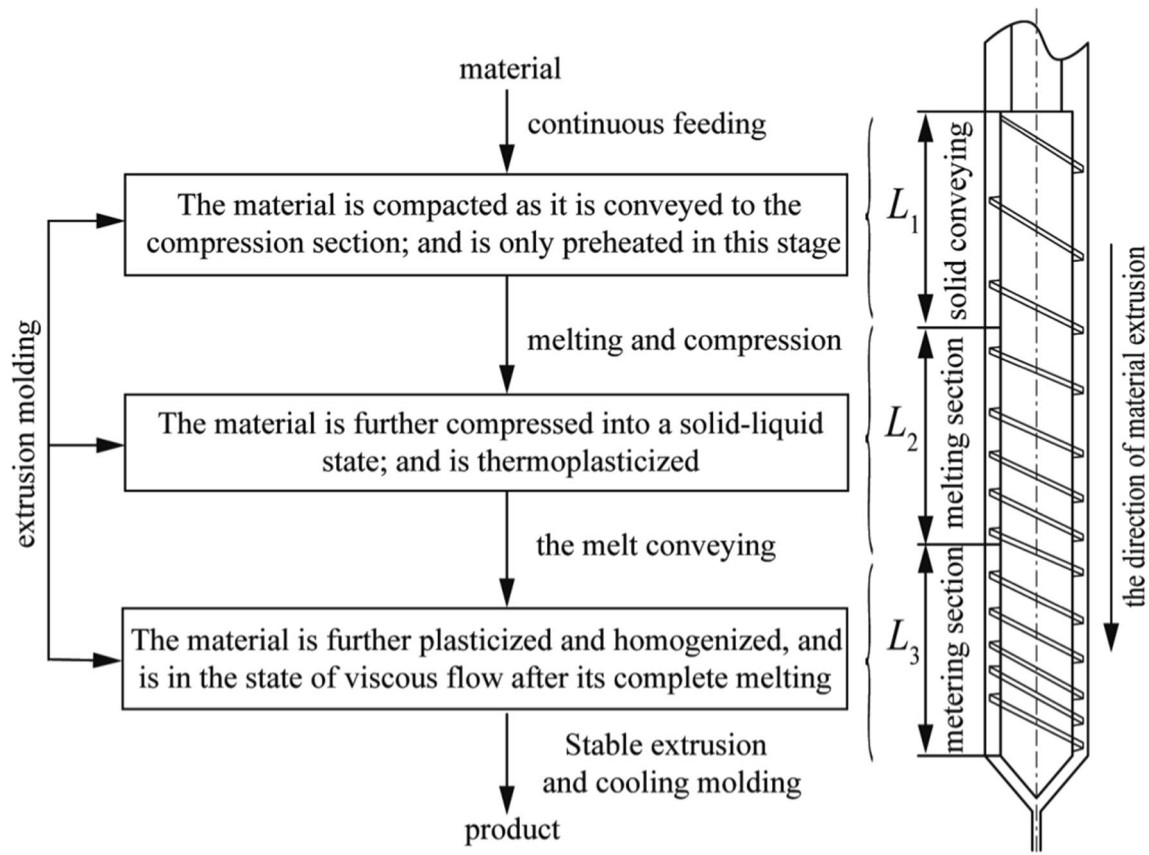


Fig. 1 The working mechanism of the new 3D printing molding equipment

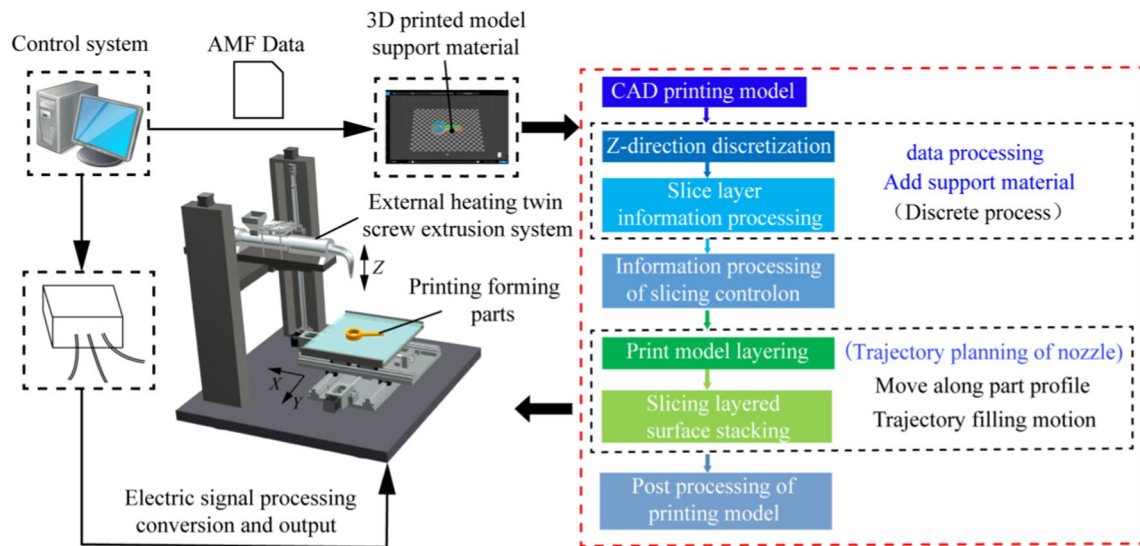


Fig. 2 The flowchart of the work system of the new 3D printing molding equipment

The numerical control system mainly completes 3D printing model slicing processing and printing equipment's electrical signal processing, conversion and output; the X–Y–Z 3D motion system mainly completes the three-dimensional molding movement of the nozzle and the printing platform; the melt extrusion system mainly completes the melt plasticizing, extrusion conveying and extrusion molding movement of the printed material. The system has a large heating range, which can be used for the extrusion of PLA (190~220 °C) and the molten plasticizing of PEEK (about 380 °C). The material can be extruded stably in the extrusion system, through the real-time regulation of the heating system and cooling system.

Determined by its working mechanism, the new screw extrusion-based 3D printing molding equipment had a molding system comprising of the numerical control zone, feed zone, and melt zone. Figure 2 outlines the flowchart of its work system.

The numerical control zone mainly consisted of a numerical control system, which completed the model's layered slicing and the equipment's electrical signal processing, conversion, and output. In the feed zone was the three-dimensional feeding system (X, Y, and Z), which accomplished the nozzle movement along the component's section contour and filling trajectory. The melting zone was mainly composed of an externally heated twin-screw extrusion system, which realized the melting plasticization, the extrusion transmission, and the extrusion molding of printing materials.

2.3 Motion Analysis for the New Type of 3D Printing Molding Equipment

The overall layout and control, as well as the transmission scheme of each moving parts, were analyzed and designed

according to the mechanism of twin-screw extrusion molding and the workflow characteristics of 3D printing molding equipment. The schematic diagram of the motion system is depicted in Fig. 3.

The motion system of this new type of 3D printing molding equipment consisted of two parts: three-dimensional feed systems along X, Y, and Z axes and a screw extrusion transmission system. The feed systems along X and Y axes completed the two-dimensional feed movement of the workbench on the horizontal plane while the Z one completed the Z direction feeding on the nozzle module. The screw extrusion transmission system completed the extrusion transmission and the extrusion molding of the materials.

3 3D Printing Molding Equipment and its Screw Structure Design

3.1 Design for the Overall Structure of the New 3D Printing Molding Equipment

This equipment follows a desktop level practical 3D printing mechanism. The mechanical system mainly consisted of three parts: feed systems along X, Y, and Z axes, a twin-screw extrusion system, and the heating and cooling system, as portrayed in Fig. 4.

A special sort of temperature-sensitive electrically-heated glass was used to prepare the workbench of the new printing equipment so that it could effectively prevent the warping deformation caused by residual stress to printing products. To ensure the efficient and accurate transmission of materials, a special cooler was equipped near the feed inlet. Moreover, the external ultrasonic vibrating device could effectively

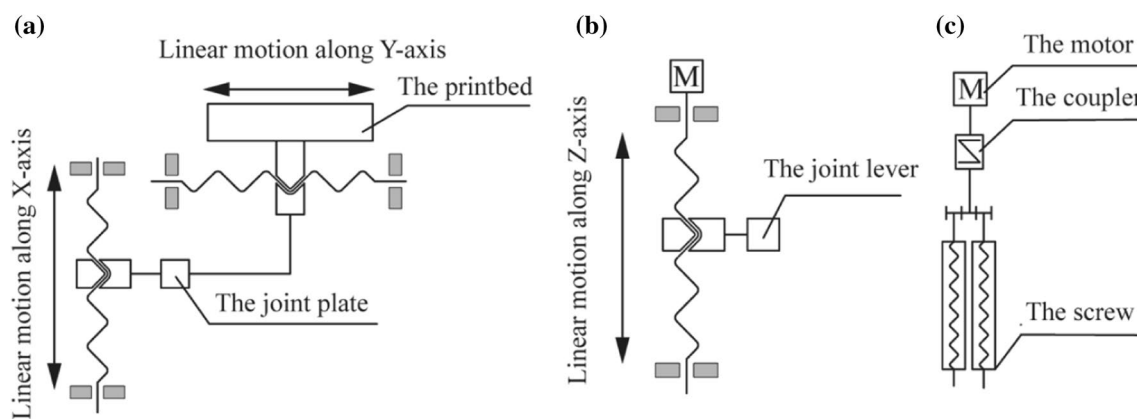


Fig. 3 Schematic diagram of motion of the new 3D printing molding equipment. **a** Feed systems along X-axis and Y-axis; **b** Feed system along Z-axis; **c** Screw extrusion transmission system 1—the foundation; 2—the stand; 3—the support plate; 4—the reducer; 5—the coupler; 6—the transmission control box; 7—the support module behind the barrel; 8—the Z-axis feed system; 9—the barrel; 10—the support

module ahead of the barrel; 11—the external connector; 12—the elbow; 13—the nozzle; 14—the workbench; 15—the Y-axis feed system; 16—the X-axis feed system; 17—the ultrasonic vibrating device; 18—the screw; 19—the heater; 20—the feed inlet; 21—the slider; 22—the guideway

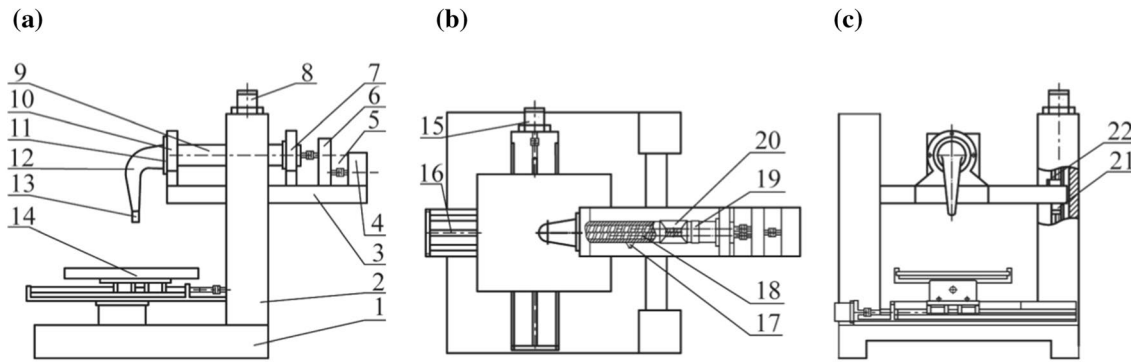


Fig. 4 Structural diagram of the new 3D printing molding equipment. a the left view; b the top view; c the front view

promote the melting and mixing of materials, essential to improve the quality of printing.

3.2 Structural Design of Screw

No such systematic design method suitable for desktop screw extrusion molding equipment was available. For the twin-screw, the performance of printing devices is directly affected by the core parts of the extrusion molding system, whether its structure and the selected parameters are reasonable. Moreover, the end face profile fundamentally determines the equipment performance in mixing, shearing, plasticization, transmission, etc. As a result, a reasonably-designed screw lies in the reasonable design of the end face profile. In this paper, each functional section of the extrusion screw was fabricated according to the end face profile of the screw module, determination processes covering the screw rotation in a correct direction, reasonable screw structural parameters, and the matching relation between the optimal twin-screw rotational speed and the printing feed rate.

3.2.1 Determination of the Rotation Direction of the Twin-Screw

The geometrical shape of threads module for self-sweeping intermeshing twin-screw are not independent of but interrelated with and influential to each other. The right screw of the twin should be processed to be left-hand threaded, rotating clockwise in view toward the machine nozzle, while the left screw should be the reverse, to ensure the normal conveying of materials toward. Figure 5 illustrates the specific counter-rotating directions of the twin screws at the same speed and the material conveying direction.

By rotating two intermeshing screws simultaneously, the forced conveying and melting mixing with positive displacement of the material in the meshing area could be achieved under the velocity difference or the flow direction change. The twin-screw extrusion system must be able to build up the head pressure high enough and to develop the motion balance between the extrusion pressure and the melt pressure [16], so as to make

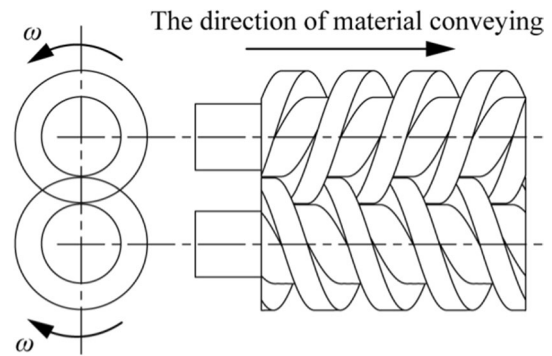


Fig. 5 Counter-rotating twin screws and the material conveying direction

the material under pressure overcome the resistance at the die. This is the only way that could extrude the materials stably and continuously at a constant temperature, pressure, and output rate by the nozzle. Thereafter, the printed products were shaped and obtained after cooling the extruded materials.

3.2.2 Design for the End Face Profile of the Screw

3.2.2.1 Design for the End Face Profile of the Thread Module for Intermeshing Twin-Screw The basic design parameters of the new screw mainly included the length-over-diameter ratio of the screw, the external diameter of the screw, and the screw pitch, etc. The relations [17] between the main dimensions are provided in Eq. (1):

$$\begin{cases} D_s - 2H = D_b \\ tg\varphi_s = T / (\pi D_s) \\ B_{ws} = B_s \cdot \cos \varphi_s \\ C_L = D_b / 2 + D_s / 2 \\ n \cdot \alpha_r + 2n \cdot \alpha_f + n \cdot \alpha_r = 2\pi \\ \cos(\alpha/2) = C_L / D_s \end{cases} \quad (1)$$

where, D_s —the screw external diameter; D_b - the screw root diameter; φ_s - the helix angle ($10^\circ \sim 30^\circ$) calculated by the external diameter; H - the channel depth; n —the number of threads; T - the thread lead; B_{ws} - the axial width of thread crest calculated by external diameter; α - the crest angle (center Angle); C_L - the center distance between two screw axes; α_t —the apex; α_r —root angle; α_f -the flank angle.

Considering that the diameter of commonly-used thermoplastic granular material is about 3 mm, and regional high temperature is conducive to thermal decomposition of material, the depth of the thread groove should not be too shallow, and the number of threads should not be too much. Therefore, a double-head screw structure was adopted in the design of this study. Analyzing the geometrical characteristics of the screw thread module and the functions and technical requirements of 3D printing, the end face profile of the desktop screw module was parameterized by the relative motion analysis [18] according to the twin-screw geometry [17]. From the relative movement principle of the twin screw as shown in Fig. 6a, the parametric equations of the end face curve of section $A_1 \sim B_1$ generated by relative motion analysis are as follows:

$$A_1 \sim B_1: \begin{cases} x = C_L \cos \omega t - R_b \cos (2\omega t - \pi/4) \\ y = -C_L \sin \omega t + R_b \sin (2\omega t - \pi/4) \\ \omega t \in [\pi/4 - \arccos (C_L/2R_b), \pi/4] \end{cases} \quad (2)$$

3.2.2.2 Rectification for the Screw End Face Profile As detailed in Fig. 6c, if the screw was directly generated by the theoretical curve of the end face, there would be a lack of meshing clearance and assembly clearance, making it difficult to carry assembly in actual processing and conducive to the dead angle in the root of the screw where material lagging occurred. This could be detrimental to the flowing, mixing, and homogenizing of materials. Therefore, rectifi-

cation was needed for the screw end face profile to ensure the normal operation of extrusion equipment.

Trapezoidal section, which is easier to be processed, was adopted to substitute the original arc section, i.e., directly replacing the arc section $A_1B_1 \sim A_4B_4$ in Fig. 6b with a straight line. At this time, the flank angle of the thread was 0. However, following the motion simulation analysis by NX software, it was revealed that some parts of the two-screw system would interfere with each other thus was unable to rotate normally, as represented in Fig. 7.

Analyzing Fig. 6b, it can be derived that the actual design needs to spare for the straight-line segment of end face curve a swing angle near the lines $A_1B_1, A_2B_2, A_3B_3,$ and A_4B_4 , to form an inclination consistent with the actual screw. The position of the straight line after swinging is highlighted in Fig. 7c $A_1B_1' \sim A_4B_4'$. According to the geometric relation between the end face curve and the thread crest in Fig. 7b and c [19], theoretical calculation and deduction helped to evaluate the range of inclination, denoted as β , as shown in Eqs. (3–5) below.

$$\beta_1 = \frac{\alpha'}{2} + \arcsin \left(M + \frac{\tan \phi_1}{\tan \theta_s} \right) \quad (3)$$

$$\alpha' = \alpha - \frac{\delta_c}{R_s \cdot \tan \theta_b} \quad (4)$$

$$M = \left(\frac{R_s}{H} - 1 \right) \sin \frac{\alpha'}{2} - \left(\frac{S}{4} - \frac{\delta_c}{2} \right) \frac{1}{H \cdot \tan \theta_s} \quad (5)$$

where, β_1 —rectified leftward swing angle of the end face curve; β_2 —rectified rightward swing angle of the end face curve; φ —the inclination of thread crest ($10^\circ \sim 15^\circ$); α' —rectified crest angle; δ_c —roll gap(0.013~0.038D).

As shown in Fig. 8, both transversal and longitudinal openings were present in the rectified twin-screw meshing

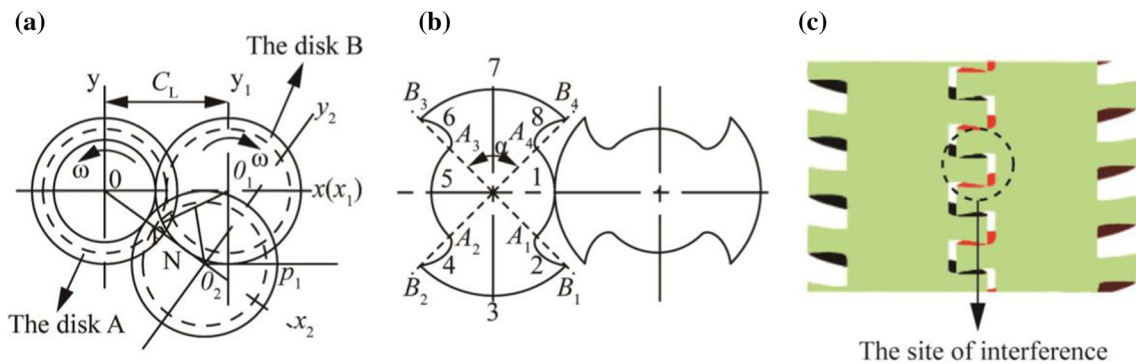


Fig. 6 Theoretical end face profile and characteristic dimensions of the twin-screw. **a** the relative movement between the twin screws; **b** the characteristic dimensions of the double-end thread module; **c**

actual state of motion θ —helix angle; α_1 —the crest angle; β —swing angle of the end face curve; α' —rectified crest angle

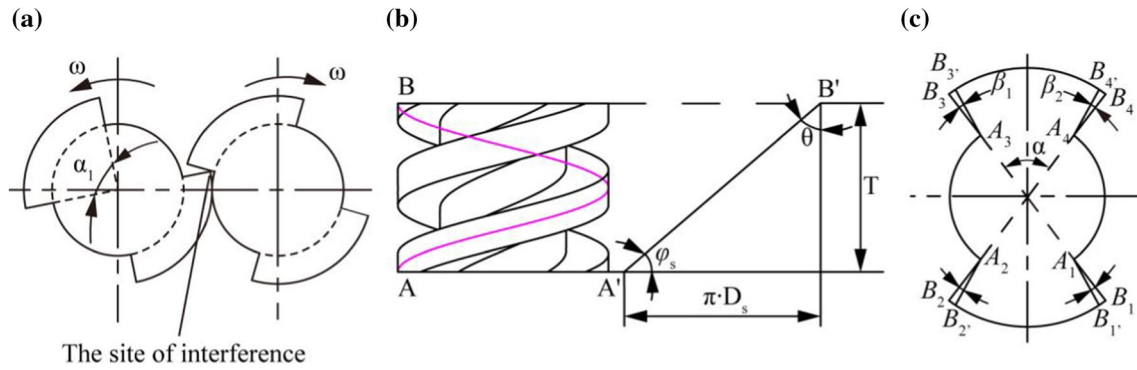


Fig. 7 Rectification of the end face curve. **a** Interference between modules of screws; **b** the unfolded drawing of the helix; **c** Geometric relation between the end face curve and the thread crest Q_t —leakage

flow through the tetrahedral clearance; Q_s —leakage flow through the side clearance; Q_c —leakage flow through the roll gaps; Q_f —leakage flow through the flight clearance

area with four types of gaps between the two intermeshing screws. Following actual assembly, no interference was observed. This guaranteed the normal operation of the twin-screw. The requirements of practical screw applications were also satisfied.

3.2.3 Design for Functional Sections of the Screw

According to the working mechanism of the new type of 3D printing molding equipment, it is prominent that the twin-screw extrusion system needs to exhibit ability not only in mixing but also in excellent conveying and pressure built-up. The mixing capacity and conveying capacity of the twin-screw extrusion system can be guaranteed by designing a reasonable end face profile of screw, while the pressure-building capacity of the twin-screw can be realized by designing the structural parameters of each section of the three-section screw.

The screw capacity in mixing and conveying could be guaranteed by the design of and following rectification to the end face profile, whereas the pressure build-up capacity by the design of the structural parameters of screw sections.

The compression ratio is an important parameter, which generally refers to the ratio of the volume of the first screw groove in the solid conveying section to the volume of the last screw groove in the metering section [20]:

$$\epsilon = \frac{\left[\frac{\pi}{4} (D_1^2 - D_{i1}^2) (T_1 - n_1 \cdot B_{1cp}) - n_1 \frac{A_1}{\cos \alpha_1} d_{1cp} \right]}{\left[\frac{\pi}{4} (D_2^2 - D_{i2}^2) (T_2 - n_2 \cdot B_{2cp}) - n_2 \frac{A_2}{\cos \alpha_2} d_{2cp} \right]} \quad (6)$$

where, ϵ —the compression ratio (1.4~4); T_1, T_2 —the screw lead in the feeding section and metering section, respectively; d_{1cp}, d_{2cp} - the axial thickness of crest in the feeding section and metering section, respectively; B_{1cp}, B_{2cp} - the width of the screw edge of the feeding section and metering section; A_1, A_2 - the area of meshing area in the feeding section and metering section, respectively; α_1, α_2 —the engagement angle in the feeding section and metering section, respectively; n_1, n_2 —the number of thread in the feeding section and metering section, respectively

As the shape and dimensions of the extrusion die of the printing equipment are determined, the pressure built by the nozzle will only depend on the material viscosity and Q , the flow of the material [21]:

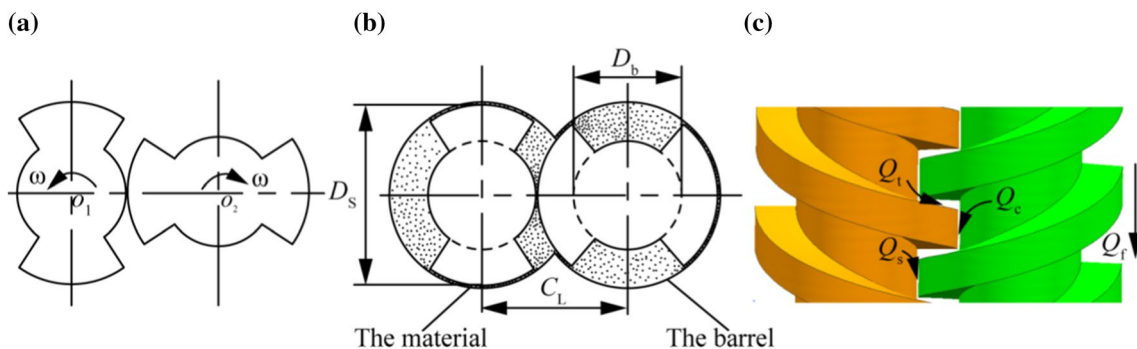


Fig. 8 Twin-screw end face profile and screw configurations. **a** rectified end face curve of screw; **b** Characteristic dimensions of the double-headed screw after rectification; **c** Sites and directions of leakage flow in the gaps

$$P = \frac{\mu}{k} Q \quad (7)$$

$$K = \frac{\pi D^2}{128(L + 4D)} \quad (8)$$

where, μ —viscosity; Q —the actual output rate of extrusion; P —the print head pressure;

k —the drag coefficient of the circular die; L —the length of the flat part of the die; D —the diameter of the die

According to Eq. (6), the capacity of the screw groove can be modified in the design of the structural parameters of screw sections, whereby realizing the compression of the material. The primary factors affecting the volume of the screw groove include its depth and pitch: the depth of the screw groove can be ascertained based on the grain diameter, while the pitch needs to be selected depending on the production capacity. The screw module with equal depth and unequal pitch outperforms that with equal pitch and unequal depth in higher production capacity and a lower stress gradient, which was favorable for a longer service life of the screw [22]. Therefore, the present study adopted the structural design with equal depth and unequal pitch to achieve the pressure build-up of the screw.

Considering the small-sized characteristics of the desktop molding equipment and in combination with the empirical length distribution of the three-section screw [23] plus other similar design theories [24], the lengths of each section of the screw were determined and are delineated in Table 1.

Major fundamental design parameters of screw modules with the equal depth and unequal pitch were estimated through the parametric design of the end face profile and are shown as follows: external diameter (D_s) 20 mm, root diameter (D_b) 12 mm, length-over-diameter ratio (L/D) 18 mm, center distance (C_L) 16.1 mm, barrel inner diameter (D_r) 21 mm, clearance between the thread crest and the barrel (δ_r) 0.5 mm. The schematic diagram is illustrated in Fig. 9. Where, S_1 —pitch of solid conveying section; S_2 —pitch of melting section; S_3 —pitch of metering section; e —width of crest; H —groove depth; D_s —external diameter of the screw; L —effective length of screw.

4 The Determination of Matching Relation

For the screw rotational speed and the feed rate of the screw extrusion-based 3D printing molding, there is a reasonable selection range for their matching. The printing quality and efficiency of the molding system can be assured only by accurate matching between the screw rotational speed and the print feed rate.

Table 1 The lengths distribution on three sections of screw

L_1 proportion of solid conveying section	L_2 proportion of melting compression section	L_3 proportion of metering section
20~30%	40~50%	30~45%
90 mm	162 mm	108 mm

4.1 Calculation of Extrusion Rate

The output of the twin-screw extrusion 3D printing molding equipment is an important parameter, and its maximum theoretical rate is attributed to the processing temperature, the variety of products, types of materials, and the structure and rotational speed of the screw. As the performance characteristics of the twin-screw largely hinge on its melt conveying characteristics, the factors associated with the performance characteristics in the melt conveying section are representative of the values of basically all corresponding performance characteristic parameters of twin-screw [25]. According to the principle of positive displacement conveying, in the engagement of inter-meshing counter-rotating twin-screw, the thread crest of one screw divides the groove of the other screw into a great many independent C-shape chambers along with the screw axis and in each chamber, the flow of the melt follows exactly the same pattern [26]. Therefore, the extrusion output rate can be calculated as the volume of material extruded per rotation of the melt conveying section and the volume of the C-shape chamber as the volume difference between a certain section of empty barrel and the corresponding screw, hence the equations as follows [27]:

$$V_1 = \left[\left(\pi - \frac{\alpha}{2} \right) R^2 + \left(R - \frac{H}{2} \right) \sqrt{\left(R \cdot H - \frac{H^2}{4} \right)} \right] S \quad (9)$$

$$V_2 = \pi \left(R - H \right)^2 S \quad (10)$$

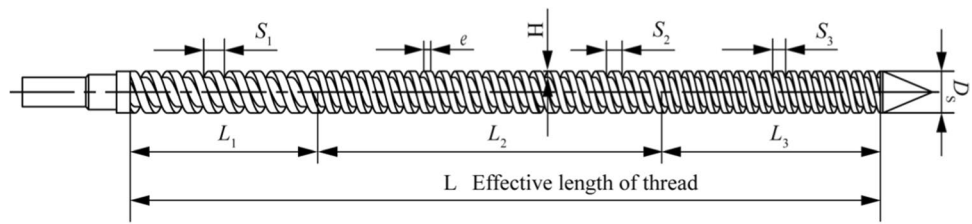
$$V_3 = 2\pi \left\{ \left(R \cdot H - \frac{H^2}{2} \right) B + \left(R \cdot H^2 - \frac{2}{3} H^3 \right) t g \phi \right\} \quad (11)$$

$$V = (V_1 - V_2 - m \cdot V_3) / m \quad (12)$$

$$V = \frac{S}{m} \left[\left(\pi - \frac{\alpha}{2} \right) R^2 + \left(R - \frac{H}{2} \right) \sqrt{R \cdot H - \frac{H^2}{4}} \right] - \pi \left(R - H \right)^2 \frac{S}{m} - 2\pi \left[\left(R \cdot H - \frac{H^2}{2} \right) B + \left(R \cdot H^2 - \frac{2}{3} H^3 \right) t g \phi \right] \quad (13)$$

Considering the relation between the screw speed and the extrusion output rate, the C-shape chamber was

Fig. 9 The schematic diagram of the screw structure



unfolded so the relation for extrusion output rate was by obtained calculus-based calculation as follows [28]:

$$Q_{\max} = \frac{N}{60} \text{tg}\phi_s (\pi D)^2 (D - C_L) \tag{14}$$

In the actual melt conveying, the impact of leakage flow should be accounted for owing to the presence of meshing clearance [29], i.e.,

$$Q_{\text{reality}} = \eta \cdot Q_{\max} \tag{15}$$

where, \$V\$—volume of C-shape chamber; \$V_1\$—half of the material volume along the length of one screw lead; \$V_2\$—volume of the root-diameter-formed cylinder along the length of one screw lead \$V_3\$—the volume of one Screw aris; \$\alpha\$—the center angle corresponding to the meshing area; \$\phi\$—flank angle; \$R\$—external radius of the screw; \$Q_{\max}\$—theoretical maximum extrusion output rate; \$N\$—rotational speed of the screw; \$D\$—screw diameter; \$Q_a\$—actual extrusion output rate; \$\eta\$—coefficient of conveying, ranging from 0.2~0.5.

It is quite evident from the above that the groove depth and the pitch size together determine the materials-conveying capacity of the screw at a given rotational speed. Upon the determined screw extrusion output rate, the pressure build-up capacity of the molding equipment’s die can be analyzed based on Eq. (7), and the screw rotational speed and the optimal screw geometric parameters can be obtained according to Eq. (9–15).

4.2 Matching of the Rotational Speed and Feed Rate

In the operation of the FDM 3D printing of molding equipment, the screw extrusion system serves as the most crucial module. As required by the quality and accuracy of printed products, material extrusion output rate, and printing feed rate need to be matched properly. At the extruding moment, the melt material from the nozzle is in the quasi-round shape, almost the same as that of the nozzle [30], and its cross-sectional area, denoted as \$S_1\$ can be expressed as:

$$S_1 = \pi \left(\frac{d}{2}\right)^2 \tag{16}$$

In the printing process, the melt material would be squeezed by both the molded object underneath and the nozzle, forming an irregular section, the effect of which turned to be a quasi-rectangle as derived from calculus-based model (Fig. 10).

Therefore, the quasi-rectangular sectional area, denoted as \$S_2\$ can be expressed as

$$S_2 = Bh \tag{17}$$

According to the Law of Conservation of Mass, the volume of material extruded by the screw per rotation is equal to the volume of material extruded from the nozzle, which is equivalent to the volume of print piled up on the print bed [31], thus:

$$V_E S_1 = V_F S_2 \tag{18}$$

$$\frac{\pi}{4} d^2 \cdot V_E = Bh \cdot V_F \tag{19}$$

After estimating the layer thickness and nozzle diameter, the relation between the feed rate and the extrusion rate can be obtained according to the requirements of the print quality:

$$\frac{V_E}{V_F} = \frac{Bh}{(\pi/4)d^2} \tag{20}$$

The screw’s rotational speed determines the material extrusion rate, which, in turn, assesses the filling rate of the nozzle. The feed system and the screw extrusion system must be highly matched to convey more materials and ensure the continuity in this process [32]. Therefore, it is necessary to state the matching relation between the print feed rate and the screw rotational speed:

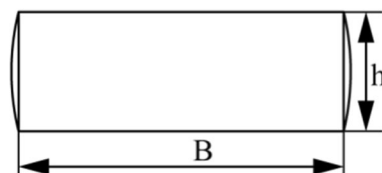


Fig. 10 The equivalent diagram of the material section

$$V = \frac{N}{60} \text{tg}\phi_s (\pi D)^2 (D - C_L) \cdot \eta = b \cdot h \cdot V_F \quad (21)$$

$$\frac{N}{V_F} = \frac{b \cdot h}{\text{tg}\phi_s (\pi D)^2 (D - C_L) \cdot \eta / 60} \quad (22)$$

where, V volume of material extruded from the nozzle; V_F —feed rate (mm/min); V_E —extrusion rate (mm/min); S_1 —sectional area of nozzle, S_2 —sectional area of filler deformed by extrusion; d —the diameter of nozzle hole; N —screw rotational speed; B —Width of the rectangular area of material section; h —layer thickness.

It can be seen from the above that the extrusion output rate can be computed from screw parameters, and the geometrical parameters directly affect the extrusion efficiency of melt. The rotational speed of the screw determines the extrusion output rate, and the precise matching relation between the extrusion rate and the feed rate provides an effective theoretical basis for the following printing process design for the screw extrusion 3D printing molding equipment.

5 Numerical Simulation of Flow Field Characteristics

The stable flow of polymeric fluid in the twin-screw extrusion system is an important prerequisite for the product to be printed and molded. The screw structural parameters, processing parameters, physical parameters, etc. which are inter-related and -affecting, are closely linked to the flowing of fluid in the passage. Therefore, in order to verify the rationality of the design for screw structure, numerical solution for the fields of pressure, viscosity, and a shear rate of the fluid in the extrusion process was obtained in isothermal transient flow under the processing conditions of double-screw rotational speed and screw lead. Furthermore, analysis and discussion were carried regarding the distribution changes of the parameters in the flow field as the screw rotates.

5.1 Development of Mathematical Modeling

Considering the complexity of material conveying conditions and flow field characteristics of screw extrusion-based 3D printing molding equipment, assumptions under ideal conditions were made regarding the fluid in the flow field for the flow field analysis:

1. The flow field was isothermal and stable;
2. The passage was filled with incompressible melt

3. The flow was laminar, three-dimensional, steady, viscous and fully developed;
4. Due to the high viscosity of the melt, the volume forces, which are far less than viscous forces, such as gravity and inertia forces, were excluded.

On the basis of the above assumptions for the isothermal field, the solution of the flow field was conducted as per the continuity equation and the equation of motion. The governing equations [33] are as follows:

the continuity equation

$$\frac{\beta'}{\eta(\gamma)} + \nabla p + \nabla \cdot v = 0 \quad (23)$$

the equation of motion [34]:

$$\begin{cases} 0 = -\frac{\partial p}{\partial x} + \left(\frac{\partial \tau_{xx}}{\partial x} + \frac{\partial \tau_{yx}}{\partial y} + \frac{\partial \tau_{zx}}{\partial z} \right) \\ 0 = -\frac{\partial p}{\partial y} + \left(\frac{\partial \tau_{xy}}{\partial x} + \frac{\partial \tau_{yy}}{\partial y} + \frac{\partial \tau_{zy}}{\partial z} \right) \\ 0 = -\frac{\partial p}{\partial z} + \left(\frac{\partial \tau_{xz}}{\partial x} + \frac{\partial \tau_{yz}}{\partial y} + \frac{\partial \tau_{zz}}{\partial z} \right) \end{cases} \quad (24)$$

the Bird-Carreau constitutive model [35]:

$$\eta(\gamma) = \eta_\infty + (\eta_0 - \eta_\infty) [1 + (\lambda\gamma)^2]^{(n-1)/2} \quad (25)$$

where, β' —coefficient of compressibility; η —apparent viscosity; γ —shear rate; V_x, V_y, V_z —velocity components along the direction of x, y, z ; p —pressure; τ_{ij} —nine stress components in the Cartesian coordinate system, in which i and j respectively denote components along x, y or z direction; η_∞ —infinite shear viscosity; η_0 —zero shear viscosity; n —the non-Newtonian index of melt; λ —the temporal parameter of Carreau Model.

5.2 Finite Element Model and Meshing

Screw modules with different lead (24 mm, 32 mm, 36 mm, and 40 mm) were selected to differentiate in their conveying capacity, pressure build-up capacity, and mixing performance from aspects of flowing and mixing. Considering the complexity in the analysis of the flow field characteristics and mixing performance, the adaptive Mesh Superimposition Technique (MST) in POLYFLOW software was adopted to subdivide the zones and moving modules through or by which the fluid flows, as shown in Fig. 11.

5.3 Boundary Conditions and Physical Parameters

Considering practicality and economy, the widely-used advanced 38CrMoAlA nitriding steel, which has excellent comprehensive performance, was chosen as the material of screw; the biodegradable polylactic acid (PLA), derived

from completely renewable raw material and pollution-free manufacturing process, thus being an ideal green polymer material, was opted as the printing material. The physical parameters of PLA are listed in Table 2 below.

The research was executed on the flow field characteristics and mixing performance of the twin-screw module based on the actual processing conditions. The boundary conditions were set as follows: the left and the right screw module were in counter-rotation and at the same speed of 10 r/min; no sliding occurred at the screw surface and the barrel inner wall; pressure boundary conditions were adopted at the inlet and outlet of the flowing passage, i.e., the inlet pressure being 0 MPa, backpressure at the outlet being 0.5 MPa.

5.4 Analysis of Melt Conveying Characteristics

5.4.1 Pressure Field

In the process of conveying evenly mixed materials in the twin-screw extrusion system, a high enough 3D printer head pressure must be established to make the extrusion pressure and the solution pressure reach dynamic balance, so that under the action of this pressure, the material can overcome the die resistance of the head and mouth, and be steadily and continuously extruded by the nozzle with constant quantitative pressure. The pressure variation trend, velocity distribution, shear rate variation and viscosity distribution of the flow field in this paper are all in accordance with the flow field characteristics of the conventional meshing anisotropic and constant velocity twin-screw, and the simulation results are consistent [17], thus proving the correctness of the numerical simulation boundary conditions in this paper.

As shown in Fig. 12a, when screw rotational speed was 10 r/min, in the cavity formed between the screw and the flow passage, the pressure on the fluid was in a stable distribution with a gradual increase along the direction of material extrusion. However, closer to the outlet, the pressure started to decrease, which largely resulted from a larger differential pressure and a more intense fluid leakage under the drag

Table 2 The physical parameters of PLA

Parameters	η_0 (Pa·s)	H_∞ (Pa·s)	λ (s)	n	ρ (Kg/m ³)
Value	2504.235	0	0.0607	0.253	1200

from the die opening at the outlet. This indicated a drop in the pressure build-up capacity of the screw at segments closer to the outlet. As shown in the Fig. 12b, the pressure in the lower meshing area demonstrating a regional high pressure was significantly higher than that in the higher meshing area. This was primarily because under the simultaneous counter-rotation of the twin screw, the materials in the extrusion system was brought into the lower meshing area and then through the roll gaps into the higher meshing area; yet the materials tended to pile in the gaps as the size of those gaps were quite small. As portrayed in Fig. 12c, there was only one phase difference between passages pressures of the left and the right screw and the difference was in a laddering increase along the extrusion direction thus creating a large pressure gradient in the end. Pressure at the outlet was stable at about 1.51 MPa. This wavelike pressure rise was mainly attributed to the fluid backflow caused by fluid pressure increased by strong extrusion at the thread crest, a process which then left a lower pressure at the crest hence the forward movement of melt. Curve corresponding to the 40 mm lead was located at the top with the strongest fluctuation, followed by those corresponding to the lead of 36 mm, 32 mm, and 24 mm. This was mainly because that screws with longer lead conveyed more fluids per unit time with a stronger extrusion, indicating that the materials were conveyed forward with positive displacement in the C-shape chamber of the counter-rotating twin screw; the screw was able to meet the requirements of pressure build-up; and as the screw lead size increased, the pressure build-up capacity of the screw improved as well in a stronger pressure fluctuation. According to Fig. 12d, when the screw lead was 32 mm, located at the top was the curve corresponding to the screw rotational speed of 5r/min, indicating that the pressure

Fig. 11 Finite element mesh. **a** the flowing zone mesh; **b** the composite mesh

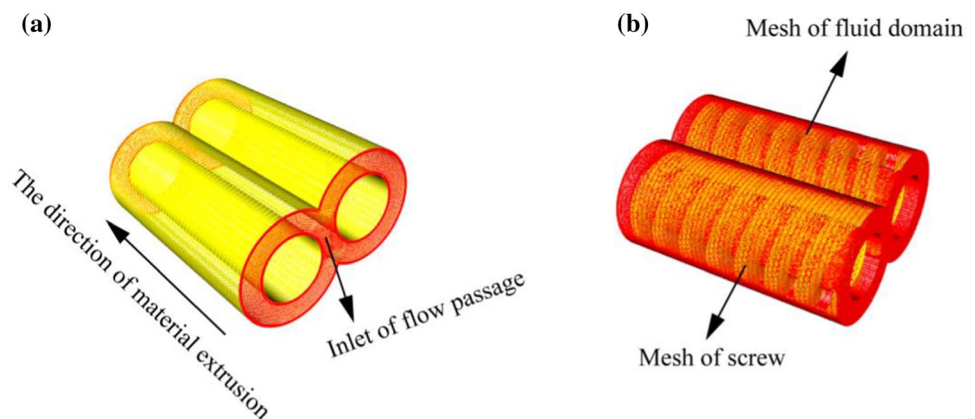
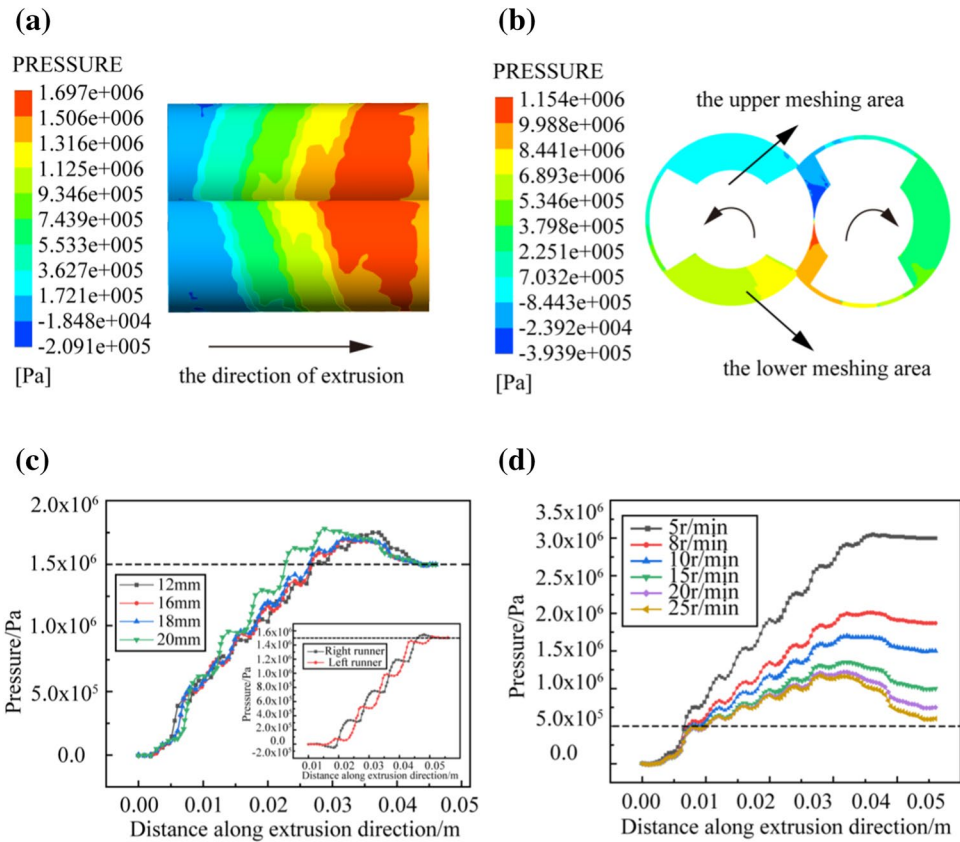


Fig. 12 The pressure distribution in the flow passage. **a** pressure distribution parallel to the axis in the flow passage; **b** pressure distribution perpendicular to the axis across the cross-section; **c** pressure distribution in the flow passage under different lead sizes; **d** pressure distribution in the flow passage under different rotational speeds



build-up capacity dropped as the screw rotated at a higher speed.

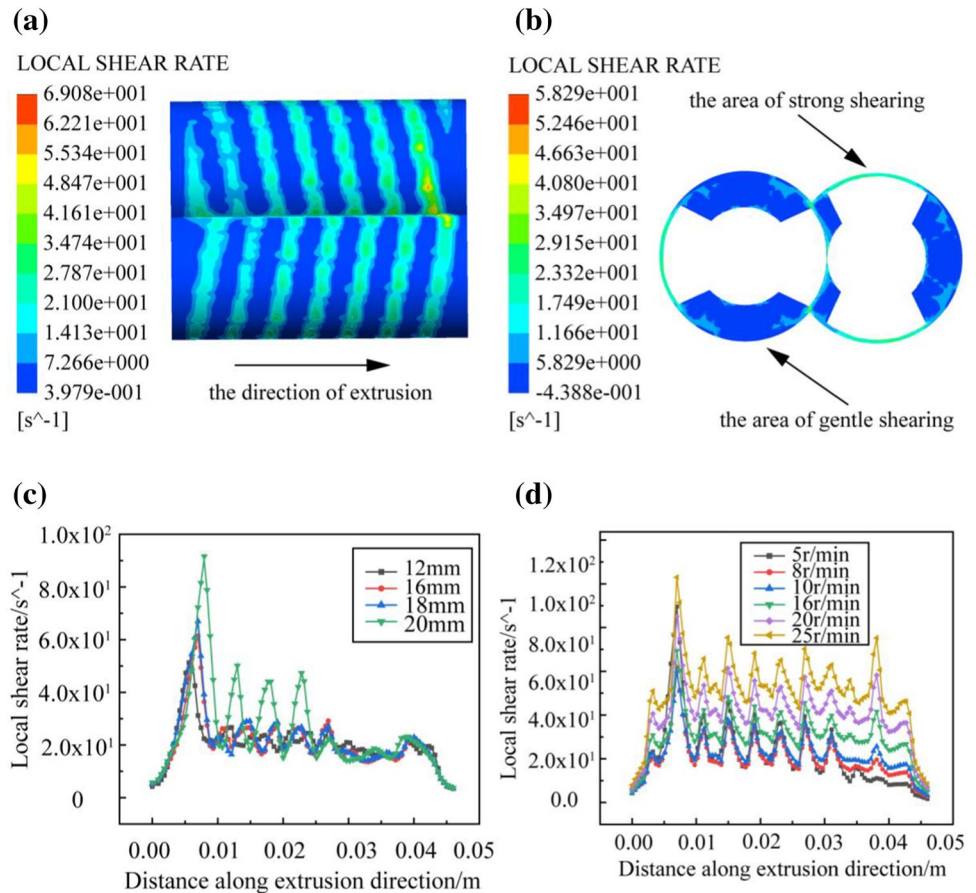
The pressure fluctuation will further result in the variation of flow rate, which is conducive to unstable extrusion, unexpected change of product size, and internal stress unevenness. The nozzle system needs to be guaranteed with not only adequate pressure build-up capacity, but also a pressure fluctuation controlled within a certain range in the flow field, to ensure the smooth extrusion of materials and the excellent performance of printed products. Therefore, the screw lead in the range of 24~36 mm were selected, not to the extent of being oversized.

5.4.2 Shear Rate Field

As highlighted in Fig. 13a, a periodic variation of the shear rate was witnessed along the extrusion direction with that at the thread crest being larger and that at the bottom of screw groove smaller. This observation could be justified by the fact that the larger velocity gradient at the thread crest brought a more violent shearing between the barrel inner surface and the thread crest, while in the screw groove the shearing was relatively gentle, reflecting a lower shearing rate. As can be perceived from Fig. 13b, the shear rate exhibited a symmetrical distribution in the screw groove with a maximum rate in the meshing area, indicating that

the material in the screw groove was subjected to a certain degree of shearing, but the strongest shearing occurred on material in the meshing area. Besides, there was a material flow from the bottom to the top in the meshing area, which signified that exchange of material between the two screws increased the probability for the material to be subjected to shearing. Figure 13c confirmed the highest peak and strongest fluctuations corresponded to the curve with the 40 mm lead located at the top, followed by the curves in the order of those corresponding to the leads of 36 mm, 32 mm, 24 mm, substantiating the fact that with the increase of screw lead size, shear rate on the materials increased as well with a more intensive fluctuation along the extrusion direction, thus favoring material mixing and compression. Figure 13d clarified that, under the same lead, shear rate corresponding to different rotational speed varied in the same trend, namely wave-like rise and fall from inlet to outlet; the downward trend became the more significant being closer to the outlet; and the shear rate was finally stabilized at about $1.0 \times 10^1 \text{ s}^{-1}$. This indicated that the material received less stronger shearing as it got closer to the exit. In addition, the highest peak value and the largest outlet shear rate of the curve corresponding to 25r/min at the top indicated that the shear rate increased with the increase of screw rotational speed, which was more favorable to plasticizing and homogenizing the material.

Fig. 13 Shear rate distribution of the flow field. **a** Shear rate field parallel to the axis; **b** Shear rate field perpendicular to the axis; **c** Shear rate distributions under different lead size; **d** Shear rate distributions under rotational speed



5.4.3 The Viscosity Field

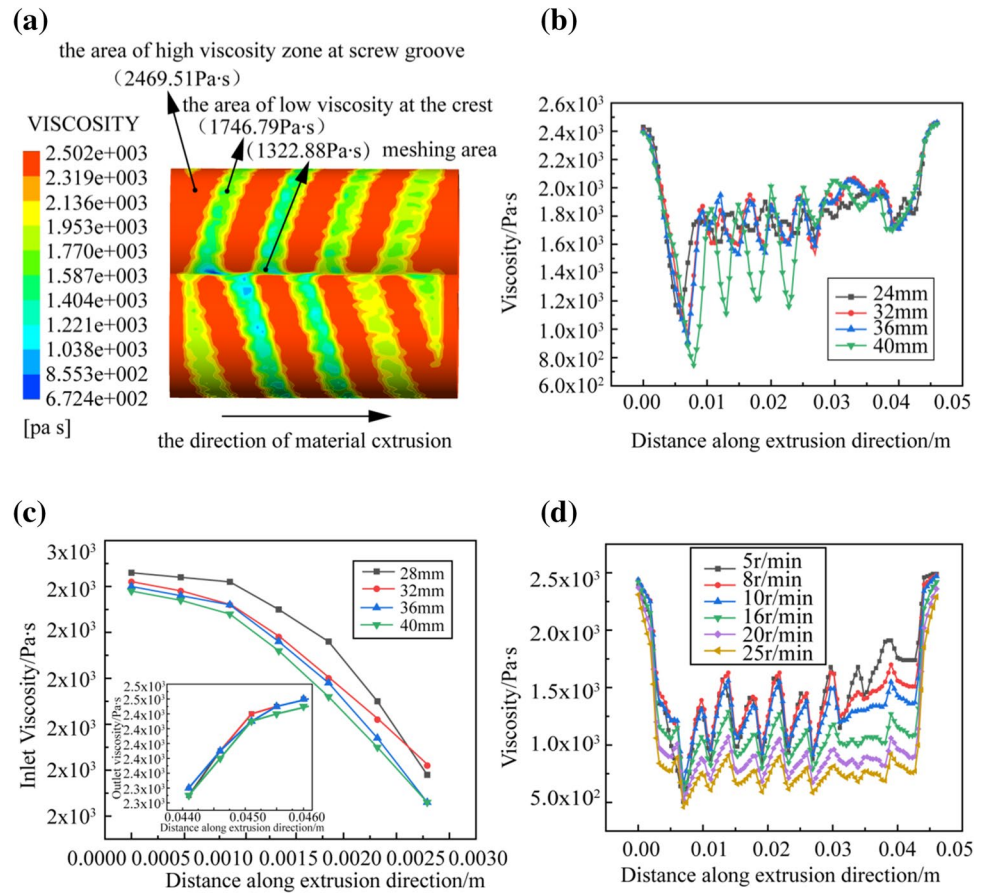
As observed in Fig. 14a, from inlet to outlet the viscosity altered in a regular pattern, with the value as high as 2469.51 Pa·s at screw groove, up to 1746.79 Pa·s at the thread crest, and only 1322.88 Pa·s in the meshing area, i.e., the viscosity dropped with the value at screw groove being the highest, that at the thread crest being the second, whereas lowest in the meshing area. This was mainly because of the rheological property of polymeric melt which meant a greater liquidity under larger velocity gradient; and that the shearing on the materials reached its highest level in the meshing area, followed by that at the thread crest being the second, and then by that at the middle of screw groove being the lowest, which two factors jointly caused the shear thinning of material and decreased the viscosity of materials with the increase of shear rate. It can be seen from Fig. 14b that the highest value of the peak represented a higher fluid viscosity in the middle of the screw groove and the lowest value of the trough represented a lower fluid viscosity at the thread crest; the closer the screw groove was to the outlet, the higher the shear rate of materials in the groove area, the lower the fluid viscosity, and in the end the better performance of the

flowing; the closer the crest was to the outlet, the greater the viscosity of the fluid near the thread crest, resulting in deterioration of the flowing performance of the fluid. It can be seen from Fig. 14c that with the increase in size of the thread lead, the viscosity at inlet and outlet decreased gradually, assisting the flow of material, therefore, the threaded module with larger lead is more favorable to the flow of material. It can be seen from Fig. 14d that the curve corresponding to a maximum rotational speed of 25r/min was located at the bottom with the lowest peak, among others, while the curve corresponding to 5r/min was located at the top with the strongest fluctuation of peak value, indicating that the viscosity dropped to be more favorable to the flowing of material as the rotational speed of screw increased.

5.4.4 Residence Time Distribution

The Residence Time Distribution (RTD) is an important indicator to characterize the mixing performance of the axial distribution. The average residence time can be used to denote the mixing time of materials, thus indirectly reflects the mixing degree of materials, as shown in Fig. 16 below.

Fig. 14 The viscosity distribution of flow field. **a** Viscosity distribution parallel to the axis; **b** Viscosity distribution under different leads; **c** Viscosity distribution at inlet and outlet; **d** Viscosity distribution at different rotational speeds



The cumulative RTD in Fig. 15a illustrates that 90% of the particles flew throughout the passage within 150 s, and during this period, the curve corresponding to 40 mm was at the bottom, followed by that corresponding to 36 mm, 32 mm, and 24 mm. The curve nearer to the top indicates that more particles flew out throughout the passage within the effective time. According to the RTD in Fig. 15b, the particle residence time corresponding to 40 mm concentrated at a few peak values of the curves on the diagram, while the residence time of 36 mm, 32 mm, and 24 mm

revealed more and more peak values. The curve corresponding to 20 mm was located on the leftmost with the narrowest distribution and the highest peak, followed by that corresponding to 36 mm, 32 mm, and 24 mm. From this, it can be concluded that the 40 mm one exhibited the shortest average retention time, among others. This could be rationalized by the fact that the thread crest of the screw with larger thread lead also faced a stronger extrusion from the material, which concentrated the forward material conveying in the groove area. As a result, the 20 mm one demonstrated the strongest

Fig. 15 Cumulative RTD and RTD. **a** the Cumulative RTD; **b** the RTD

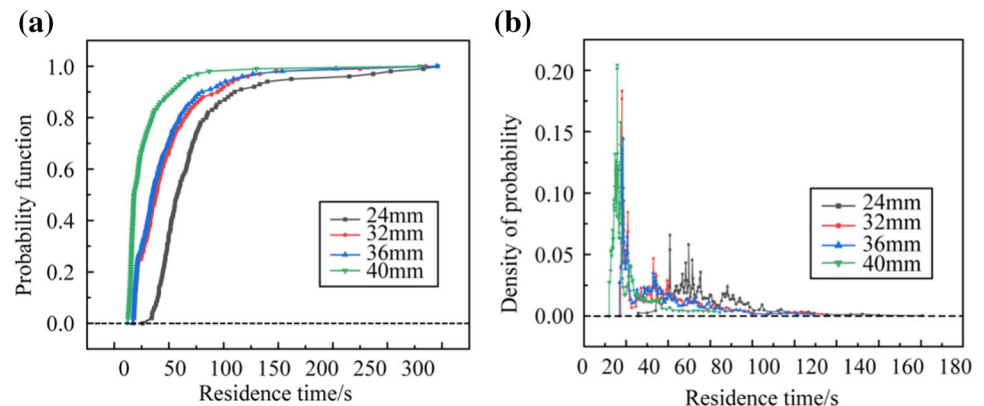
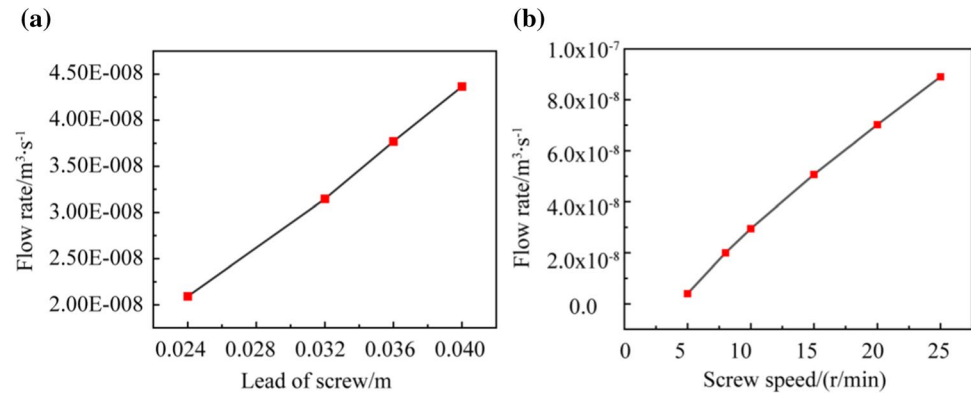


Fig. 16 Relation between the lead of screw/screw speed with extrusion output rate. **a** the influence of lead of screw on outlet flow rate; **b** the influence of screw speed on outlet flow rate



conveying capacity. It can be thus seen that the screw with a longer thread lead has a higher conveying capacity. In the practical application of production, the thread with properly short lead can be selected to improve the axial mixing performance.

5.4.5 Extrusion Characteristic

Figure 16a illuminated the largest volumetric flow rate corresponding to 0.04 m lead, followed by the 0.036 m, the 0.032 m, and the 0.024 m, indicating that as the lead size became larger, the screw also demonstrated a higher axial conveying capacity, thus a larger flow rate at the passage outlet. Therefore, the material conveying capacity of the screw can be increased by applying threaded modules with a larger lead size in the feeding section of the extrusion screw. Figure 16b reveals that the screw conveying capacity demonstrated a linear increase with the increase of screw speed, indicating that the axial velocity of the forward conveying with positive displacement was proportional to the screw rotational speed. This was also in accordance with the matching relation between the screw rotational speed and feed rate mentioned above in Eqs. (21), (22), which further verified the accuracy of the velocity matching relation.

6 Conclusion

This paper designed a new type of desktop 3D printing molding equipment based on the screw extrusion technology and the working mechanism of 3D printing molding. The flow field distribution of materials throughout the screw's melt conveying section was explored with both theoretical calculation and numerical simulation. In the end, the rationality in the structural design of the twin-screw, which serves as the core module, was verified as a conclusion:

In view of the current lack of systematic twin-screw design methods suitable for desktop-level FDM-type 3D

printing extrusion molding, and the current various types of counter-rotating intermeshing twin-screw end-face profile mathematical models are inconsistent, performance optimization and comparative analysis are difficult, etc., Established a mathematical model based on the design of the twin-screw end profile of the 3D printing molding system, and gave the relevant formulas for calculating the geometric characteristics of the screw, and gave the mathematical model of the screw extrusion volume and various structural parameters, The best matching model of the screw speed and the movement speed of the 3D printing nozzle is given.

By controlling the screw speed and related geometric parameters, the quantitative control of nozzle extrusion flow can be realized, which can be used to formulate the molding process standard based on screw extrusion 3D printer. As long as the control parameters are changed, the control of different printing accuracy can be realized; by parametrically changing the screw end profile, the twin-screw suitable for extruding different materials can be designed, It can be used to guide the parametric design, screw end surface profile evolution design and performance analysis of functional screw for serial 3D printer.

This new type of screw extrusion-based 3D printing molding equipment realized the optimization from industrial grade to the relatively small-sized and more convenient desktop type. This innovated low-cost equipment is compact and simple in its overall structure and is convenient to operate; can overcome the current limitation in material selection faced by 3D printing equipment; can avoid secondary material melting; is adaptive to processing systems for different materials; can print from materials that were either pure or hybrid, powdery or granular. In conclusion, this newly designed equipment is suitable for rapid prototyping, particularly for green manufacturing.

A desktop intermeshing twin screw with equal speed, equal groove depth, and the unequal pitch was designed by parameterization, which filled the gap that there had been no systematic design method suitable for the desktop screw. Through the analysis of the relation between screw

parameters and rotational speed in the 3D printing molding system, the matching relation between the rotational speed of screw and feed rate of the nozzle under actual operation was obtained: layer thickness (h), 0.25 mm; the width of the cross-section of material (B), 0.4 mm; the range of screw rotational speed ($N_{\max} \sim N_{\min}$), 15~8 r/min; the range of feed rate ($V_{F\max} \sim V_{F\min}$), 1403.33~746.24 mm/min. The determination of the optimal matching relation ensures the stability of the printed model quality and the printing efficiency of the molding system.

The volumetric flow rate at the outlet derived from theoretical calculation $3.51 \times 10^{-8} (\text{m}^3/\text{s})$ was close to the value from simulation ($3.18 \times 10^{-8} (\text{m}^3/\text{s})$), indicating that the material can be extruded at a constant output rate. The outlet pressure derived from the theoretical calculation (1.48 MPa) was close to the simulation value of 1.51 MPa, indicating that the screw system can meet the requirements of pressure build-up in processing. The flow rate at the outlet was proportional to the screw rotational speed, which was consistent with the theoretical analysis of the extrusion output rate, thus verified the reliability of the results. The axial mixing capacity decreased as the screw lead size increased, which was in agreement with that in actual operation, indicating that the structural design of the screw was reasonable.

At the same rotational speed, with the increase of the screw lead size, the shear rate at inlet increased gradually, viscosity at the inlet section decreased gradually, and the axial flow velocity increased. However, the pressure fluctuation became more intensive, which was not favorable to the stability of extrusion. Therefore, the lead within the range of 24~36 mm is suitable to be selected for the application in actual production.

With the thread lead kept constant, and the rational speed decreased, the screw demonstrated a higher capacity of pressure build-up and a stronger pressure fluctuation at the outlet. However, if the rotational speed became so low that it decreased the shear rate, it can become unfavorable to the plasticization and homogenization of materials, which was conducive to the drop in intermolecular forces of materials and would weaken the mechanical strength. When the screw speed became excessively high, as the motor load increased, it could cause instability in the pressure at the nozzle and of the output rate, which would further affect the molded quality of the print. Therefore, in actual production, the screw rotational speed should be selected within a reasonable range of 8~15r/min according to specific working conditions, so that the material could be extruded from the nozzle at a stable output rate and pressure.

As the screw lead size increased, the average cumulative residence time of the material decreased, and the axial mixing performance dropped, but in return, the conveying capacity of the thread module improved. The thread module with properly short lead can be selected to extend the

residence time of the material, so as to improve the axial mixing performance.

As the lead and rotational speed of screw modules were altered, the melt flows in the passage under different parameters were simulated to analyze the influence characteristic of the change in lead size and rotational speed on the flow fields. This paper not only obtained the optimized parameters of speed and lead but also verified the results of the simulation and the rationality in the structural design for the twin-screw module. Overall, this study highlighted the practicability of this new type of screw extrusion-based 3D printing molding equipment, thus has provided a certain theoretical basis for the design of a serialized functional screw extrusion system.

Funding This work was supported by Natural Science Basic Research Plan in Shaanxi Province of China (2021JM-486); National Natural Science Foundation of China (51703121); Nature Foundation of Shaanxi Province (2019JM-267); Postgraduate Innovation Fund Project of Shaanxi University of Science and Technology (SLGYCX2028).

Data Availability The datasets generated during and/or analyzed during the current study are available from the corresponding author on reasonable request.

Declarations

Conflicts of interest The authors declare that they have no conflict of interest.

References

- Gao, W., Zhang, Y., Ramanujan, D., Ramani, K., Chen, Y., Williams, C. B., Wang, C. C., Shin, Y. C., Zhang, S., & Zavattieri, P. D. (2015). The status, challenges, and future of additive manufacturing in engineering. *Computer-Aided Design*, 69, 65–89.
- Singh, R., & Garg, H. K. (2016). Fused deposition modeling—a state of art review and future applications. *Reference Module in Materials Science and Materials Engineering*. <https://doi.org/10.1016/B978-0-12-803581-8.04037-6>
- Tseng, J.-W., Liu, C.-Y., Yen, Y.-K., Belkner, J., Bremicker, T., Liu, B. H., Sun, T.-J., & Wang, A.-B. (2018). Screw extrusion-based additive manufacturing of PEEK. *Materials & Design*, 140, 209–221.
- Thermwood. (2018). Thermwood unveils new 3d print head design. <http://additivemanufacturing.com/2017/05/25/thermwood-unveils-new-3d-print-head-design/>. Accessed 29 May 2018.
- Silveira, Z. C., Freitas, M. D., Neto, P. I., Noritomi, P. Y., & Silva, J. (2014). Study of the technical feasibility and design of a mini head screw extruder applied to filament deposition in desktop 3-d printer. *Key Engineering Materials*, 57, 151–154.
- Kong, T., Stone, H. A., Wang, L., & Shum, H. C. (2018). Dynamic regimes of electrified liquid filaments. *Proceedings of the National Academy of Sciences*, 115(24), 6159–6164.
- Hu, D., & Chen, J. (2005). Meshing direction twin-screw extruder screw combination in the performance of the numerical study (II) feature analysis. *Chinese Plastics*, 12(6), 103–109.

8. Orefice, L., & Khinast, J. (2017). DEM study of granular transport in partially filled horizontal screw conveyors. *Powder Technology*, 305, 347–356.
9. Villmow, T., Kretschmar, B., & Pötschke, P. (2010). Influence of screw configuration, residence time, and specific mechanical energy in twin-screw extrusion of polycaprolactone/multi-walled carbon nanotube composites. *Composites Science and Technology*, 70(14), 2045–2055.
10. Sarhangi Fard, A., Hulsen, M. A., Meijer, H. E., Famili, N. M., & Anderson, P. D. (2012). Tools to simulate distributive mixing in twin-screw extruders. *Macromolecular Theory and Simulations*, 21(4), 217–240.
11. Aslanzadeh, S., Saghlatoon, H., Honari, M. M., Mirzavand, R., Montemagno, C., & Mousavi, P. (2018). Investigation on electrical and mechanical properties of 3D printed nylon 6 for RF/microwave electronics applications. *Additive Manufacturing*, 21, 69–75.
12. Wang, S., Badarinath, R., Lehtihet, E.-A., & Prabhu, V. (2017). Evaluation of additive manufacturing processes in fabrication of personalized robot. *International Journal of Automation Technology*, 11(1), 29–37.
13. Spackman, C. C., Frank, C. R., Picha, K. C., & Samuel, J. (2016). 3D printing of fiber-reinforced soft composites: Process study and material characterization. *Journal of Manufacturing Processes*, 23, 296–305.
14. Lunetto, V., Priarone, P. C., Galati, M., & Minetola, P. (2020). On the correlation between process parameters and specific energy consumption in fused deposition modelling. *Journal of Manufacturing Processes*, 56, 1039–1049.
15. Rackl, M., & Günthner, W. A. (2016). Experimental investigation on the influence of different grades of wood chips on screw feeding performance. *Biomass and Bioenergy*, 88, 106–115.
16. Geng, P., Zhao, J., Wu, W., Ye, W., Wang, Y., Wang, S., & Zhang, S. (2019). Effects of extrusion speed and printing speed on the 3D printing stability of extruded PEEK filament. *Journal of Manufacturing Processes*, 37, 266–273.
17. Wei, J., & Zhang, G. (2018). *Design theory and method of profile of screw element for twin-screw kneade*. Beijing: Science Press.
18. Wei, J., Sun, X., & Sun, W. (2013). Design and numerical simulation of rotor profile of twin-screw kneader. *Journal of Mechanical Engineering*, 49(3), 63–73.
19. Song, J., & Feng, L. (2004). Research and application of conical twin-screw 3d solid modeling. *China Plastics*, 45(6), 102–108.
20. Geng, X. (2003). *Twin screw extruder and its application*. Beijing: China Light Industry Press.
21. Qin, J. (2016). *Research on symmetrical mesh twin screw 3D food printer*. Nanning: Guangxi University.
22. Wang, Y., Fang, Y., & Niu, X. (2014). Optimal matching relationship between screw speed and feed speed in 3D printing process. *Journal of Qingdao University (Natural Science edition)*, 27(3), 53–57.
23. Zhu, F. (2001). *Extrusion theory and application*. Beijing: Light Industry Press.
24. Yi, X. (1997). *Preparation and processing of polymer materials*. Hangzhou: Zhejiang University Press.
25. Liu, H., & Liu, J. (1994). Approximate analytic Solution of melt conveying flow field and characteristics of meshing Hetero-rotating twin screw extruder. *Synthetic resins and plastics*, 5(4), 35–40.
26. Liu, H., & Lv, B. (1995). Analytical method is used to approximate the transmission behavior of meshing hetero-twin screw melt. *Special rubber product*, 8(4), 33–37.
27. Liu, H., & Liu, J. (1994). Approximate solutions for melt-conveying flow field and melt-conveying performances of a closely intermeshing counter-rotating twin-screw extruder[J]. *China Synthetic Resin and Plastics*, 1, 51–59.
28. Liu, H., & Liu, J. (1994). Approximate analytical solution of flow field and characteristics of melt conveying in intermeshing counter rotating twin screw extruder. *Synthetic Resins and Plastics*, 04, 35–40.
29. Yang, L., Rui, M. A., Huang, B. D., & Yun-Long, X. U. (2017). Study on application and design of extrusion screw for fdm 3d printing. *Foundry Equipment & Technology*, 03, 8–10+15.
30. Xue, S. H., Yang, F. C., & Bai-Yuan, L. V. (2007). Comparative analysis on rubber extruder screw strength based on Pro/E and ANSYS[J]. *Journal of Qingdao University of Science and Technology (Natural Science Edition)*, 02, 155–157.
31. He, X., Pan, X., & Liu, X. (2006). Compensation of measurement on fused deposition modeling. *Machinery & Electronics*, 4, 70–72.
32. Wang, C., Wang, H., & Chao, Y. (2018). Modal analysis and optimization design of extruder screw for powder feed 3D printer. *Plastics Industry*, 46(3), 47–50.
33. Wei, J., Liang, X. L., & Chen, D. (2014). Evolution of rotor profile and its mixing performance of dual screw extruder. *Chinese Journal of Mechanical Engineering*, 50(15), 34–44.
34. Tao, W. (2001). Numerical heat transfer. Xi'an: Xi'an Jiaotong University Press.
35. Bi, C. (2018). *Polyflow software foundation and its application in twin screw extrusion simulation process*. Beijing: Mechanical Industry Press.

Publisher's Note Springer Nature remains neutral with regard to jurisdictional claims in published maps and institutional affiliations.



Haiqing Bai Professor of Shaanxi University of technology, Dean of School of mechanical engineering, famous teaching teacher of Shaanxi Province, academic leader of mechanical engineering in key disciplines of Shaanxi Province, member of intelligent manufacturing professional committee of China Society of mechanical engineering, senior member of China Society of mechanical engineering, and director of Shaanxi society of mechanical engineering. He is a member of the Teaching Committee of mechanical design, manufacturing and Automation Discipline of China Machinery Industry Education Association and the academic committee of Shaanxi University of technology. At present, he has published more than 90 academic papers.



Wang Qin once studied in the school of mechanical engineering of Shaanxi University of technology, is an academic master. His main research direction is digital and green intelligent manufacturing technology. He has participated in the research group, the National Natural Science Foundation of China and the natural science foundation of Shaanxi Province. He has won many scholarships such as national scholarship for graduate students, national inspirational scholarship, Internet plus manufacturing, innovation and creative competition, and has published more than 16 academic papers.



Shikui Jia received the Ph.D. degree in materials processing engineering from South China University of Technology (SCUT), Guangzhou, China, in 2014. He is currently an associated professor of School of Materials Science and Engineering, Shaanxi University of Technology. He has authored or coauthored more than 40 academic papers and article in journals and conferences in the past five years. His research interests include polymer in advanced technologies, polymer materials microstructure and properties.



Yiwei An once studied in Shaanxi University of technology and master of mechanical engineering, mainly engaged in digital manufacturing and laser melting technology.



Li Ren a graduate student of Mechanical Engineering School of Shaanxi University of technology. His main research direction is digital manufacturing and polymer simulation processing technology.



Jun Bao a graduate student of Mechanical Engineering School of Shaanxi University of technology. His main research interests are digital manufacturing and laser selective melting technology.